Available online at www.sciencedirect.com
SCIENCE DIRECT®
Thermochimica Acta 403 (2003) 105–114
thermochimica acta
www.elsevier.com/locate/tca

Interrelation between side chain crystallization and dynamic glass transitions in higher poly(*n*-alkyl methacrylates)

Elke Hempel, Heiko Huth, Mario Beiner*

Fachbereich Physik, Universität Halle, 06099 Halle/Saale, Germany

Received 5 November 2002; received in revised form 10 February 2003; accepted 14 February 2003

Abstract

Calorimetric and dielectric results for crystallizable poly(*n*-alkyl methacrylates) (PnAMA) with $C = 12$, 16 and 18 alkyl carbons per side chain are presented. Degree of crystallization D_{cal} and melting peak temperature T_M are estimated from conventional DSC measurements. For poly(*n*-hexadecyl methacrylate) ($C = 16$) the influence of isothermal crystallization is studied by DSC as well as TMDSC. Changes in dielectric relaxation strength $\Delta\varepsilon$ and α peak shape during crystallization are investigated. Effects of side chain crystallization on the complex dynamics of PnAMA are discussed. The results are related to the relaxation behavior of lower nanophase-separated PnAMA with two co-existing glass transitions, the conventional glass transition (a or α) and the polyethylene-like glass transition (α_{PE}) within alkyl nanodomains formed by aggregated alkyl rests. It is shown that amorphous as well as semicrystalline PnAMA can be understood as nanophase-separated polymers with alkyl nanodomains having a typical dimension of 1–2 nm. The results are compared with the predictions of simple morphological pictures for side chain polymers. X-ray scattering data for the amorphous and semicrystalline PnAMA are included in the discussion. Common aspects of nanophase-separated systems in both states as well as differences caused by crystallization are discussed. Indications for the existence of rigid amorphous regions are compiled. Different approaches to explain a similar increase of $T_g(\alpha_{PE})$—the glass temperature of the amorphous alkyl nanodomains—and T_M—the melting temperature of crystalline alkyl nanodomains—with side chain length are considered. Pros and cons of both approaches, based on increasing order within the alkyl nanodomains and confinement effects in nanophase-separated systems, are discussed. Main trends concerning crystallization and cooperative dynamics are compared with those in other systems with self-assembled nanometer confinements like microphase-separated blockcopolymers or semicrystalline main chain polymers.

Keywords: Poly(*n*-alkyl methacrylates); Crystallization; Glass transition; Calorimetry; Dielectrics

1. Introduction

Crystallization behavior and dynamics of side chain polymers with long alkyl rests have been investigated since the early years of polymer research by dilatometry and calorimetry [1,2], different methods of relaxation spectroscopy [3–5], and scattering techniques [6]. This topic is related to other important fields of polymer research and application like the optimization of widely used semicrystalline polymers, development and design of liquid crystalline materials or a better understanding of the complex dynamics in biological systems.

A lot of work was done on linear polymers with lamellar crystals intercalated by less ordered regions [7,8]. It was shown that the dynamics in the amorphous regions of such semicrystalline polymers differs

* Corresponding author. Tel.: +49-3455525350; fax: +49-3455527017.
E-mail address: beiner@physik.uni-halle.de (M. Beiner).

0040-6031/03/$ – see front matter © 2003 Elsevier Science B.V. All rights reserved.
doi:10.1016/S0040-6031(03)00098-4

significantly from those in purely amorphous materials due to restrictions by the crystalline regions [9–11]. Usually, the dynamic glass transition α broadens due to crystallization and T_g shifts to higher values [12]. Dielectric investigations in the molten and semicrystalline state showed in many cases a decrease of the dielectric relaxation strength during the crystallization accompanied by a shift of the average relaxation frequency of the broadened α relaxation to lower values [10,11]. Similar behavior was observed recently also for side chain polymers [13,14] although sometimes no shift of the α relaxation frequency occurs [14].

In the recent time new impulses come also from the increasing interest in nanophase-separated materials [15], a renewed discussion about the basics of polymer crystallization [16] and a lot of questions related to crystallization [17] and cooperative dynamics [18,19] in nanometer confinements.

Nanophase separation effects with typical length scales in the 1–5 nm range are obviously a typical feature of amorphous and semicrystalline materials with incompatible molecule parts [15]. Interesting examples are polymers with long alkyl rests in the side chain showing a nanophase separation of incompatible main and side chain parts [20]. It was shown recently for a series of amorphous poly(n-alkyl methacrylates), PnAMA, that there are structural as well as dynamic indications for the nanophase separation [24]. (I) In X-ray scattering data for higher PnAMA, a pre-peak in the range $2\,\mathrm{nm}^{-1} < q < 5\,\mathrm{nm}^{-1}$ was observed (inset of Fig. 1A). This pre-peak shifts systematically to lower scattering vectors q with increasing side chain length indicating an increase of the repeating unit from an Bragg approximation $d_{\mathrm{II}} = 2\pi/q_{\max}$ in the 1–3 nm range (Fig. 1A). Obviously, alkyl rests belonging to different monomeric units and chains aggregate in the melt and form larger and larger alkyl nanodomains. (II) Similar to the situation in microphase-separated block copolymers nanophase-separated polymers with long alkyl rests show two co-existing glass transitions. The conventional glass transition (α) involving the main chain and an additional polyethylene-like glass transition (α_{PE}) within the alkyl nanodomains.[1] This can

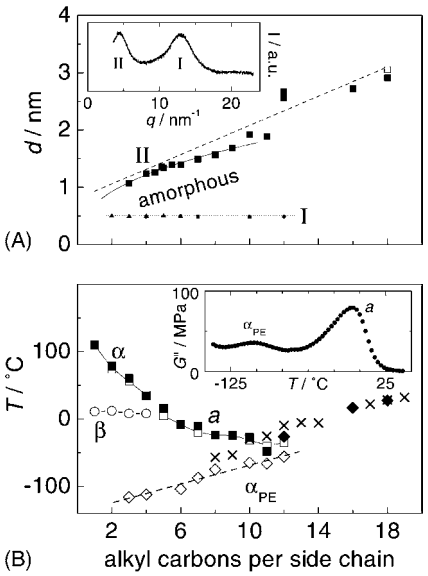

Fig. 1. Structural and dynamic parameters for PnAMA as function of the number of alkyl carbons per side chain. (A) Equivalent Bragg spacings for a series of amorphous PnAMA including random copolymers (■) and semicrystalline poly(n-octadecyl methacrylate) (□) as obtained from SAXS at $T = 25\,^{\circ}\mathrm{C}$ (for details see [22]). WAXS data by Miller et al. [6] (▲) and Floudas and Stepanek [21] (●) are included. The dashed line indicates the slope for an all *trans* configuration of the alkyl rests. The X-ray scattering intensity for poly(n-heptyl methacrylate) is given in the inset. Pre-peak (II) and conventional van der Waals peak (I) are indicated. (B) Peak maxima from $G''(T)$ shear curves at 10 rad/s ((□) a or α, (◇) α_{PE}, (○) β) and from c_p'' TMDSC curves at $t_p = 60\,\mathrm{s}$ (■) for amorphous PnAMA and melting temperatures for semicrystalline PnAMA (◆) as well as alkanes (×) [23]. The inset shows the G'' curve for poly(n-hexyl methacrylate) ($C = 6$) at 10 rad/s with co-existing a and α_{PE} peaks.

be concluded from data of the 3ω method of heat capacity spectroscopy in combination with those from other relaxation spectroscopy methods. The α_{PE} process is observed in dynamic heat capacity (c_p^*) and shear (G^*) data while the α_{PE} contributions to the dielectric response (ε^*) are negligible [25]. Calorimetric measurements by DSC on this [26] and other polymer series [27,28] support this picture.

An interesting aspect seems to be the interrelation between the complex dynamics in such nanophase-separated systems and side chain crystallization. In other words, the question is what happens with the *two* dynamic glass transitions in side chain polymers if long and flexible alkyl rests crystallize within the

[1] Note, that the α, β, γ nomenclature used here is different from that used for semicrystalline polymers like polyethylene, where α belongs to crystal effects, β is the cooperative glass transition and γ belongs to localized, less or non-cooperative motions.

alkyl nanodomains formed due to self-assembling in the melt. Note, that there is a systematic increase of the relaxation temperature (or T_g) of the α_{PE} process with side chain length (Fig. 1B). This trend could be due to an increase of order within the alkyl nanodomains consistent with pre-ordering effects [16] or could be related to restrictions of the cooperative motions by the size of the alkyl nanodomains being a self-assembled confinement for the α_{PE} process in such systems [25]. Related questions are those for rigid amorphous regions in semicrystalline materials [29,30] and the controversially debated question for existence and size of cooperatively rearranging regions (CRRs) in glasses [31–34]. Moreover, one can expect contributions to a better understanding of the dynamics and the properties of confined or semicrystalline materials—like the widely used polyolefines—with a lot of internal restrictions.

We present here a systematic study of the crystallization in higher PnAMA by standard and temperature-modulated DSC in combination with dielectric spectroscopy measurements on selected PnAMA samples. The aim is to learn more about the transition from amorphous nanophase-separated side chain polymers to semicrystalline materials with oriented alkyl rests and the influence of the crystallization process on the complex dynamics of these systems.

2. Experimental

The poly(*n*-alkyl methacrylates) with $C = 10$, 12 and 18 were synthesized by standard free-radical polymerization. Poly(*n*-hexadecyl methacrylate) ($C = 16$) was purchased from Aldrich as a solution in toluene. All samples have high molecular weight ($\bar{M}_w > 10^5$ g/mol) and similar tacticity (≈78% syndiotactic diades). Table 1 summarizes the characteristica of the used poly(*n*-alkyl methacrylates).

For the calorimetric measurements a DSC 7 instrument (Perkin-Elmer) with temperature modulated DSC (TMDSC) software-option was used. The sample mass for DSC and TMDSC measurements was about 10–15 mg. The DSC was calibrated at zero heating rate according to the GEFTA recommendation [35]. The calibration was checked in the TMDSC mode with the smectic A to nematic transition of the liquid crystal 8OCB [36,37]. Nitrogen gas with a flow rate of about 20 ml/min was purged through the cell. TMDSC measurements are performed with saw-tooth-like modulation. Details of the data evaluation methods are described in [38]. Multi-frequency TMDSC measurements are performed according to [39] in order to get some additional information about c_p^* at higher frequency. Fourier components, which occur during a special step-like heating program, are analyzed in these experiments.

For dielectric measurements, we used a commercial setup from Novocontrol with a Schlumberger SI1260 response analyzer. The sample was prepared in a cell with an electrode diameter of 20 mm and a sample thickness of 0.1 mm. The measurements were done in temperature-step-scan mode. At each temperature, the complex dielectric function $\varepsilon^*(\omega) = \varepsilon' - i\varepsilon''$ was scanned in the frequency range from 0.1 Hz to 1 MHz. A cooling experiment with temperature steps of 1 K corresponding to effective rate of −0.1 K/min was performed on PnHDMA ($C = 16$). A second

Table 1
Sample characterization and comparison of dielectric and calorimetric results for higher poly(*n*-alkyl methacrylates)

C	Label	Full name	M_0 (g/mol)	$\bar{M}_w$ (kg/mol)	$\bar{M}_w/\bar{M}_n$	T_M[a] (°C)	ΔH (J/g)	ΔH (kJ/mol)	D_{cal}[b] (mol%)[c]	D_ε (%)	$C_{crystal}$[d]	$C_{non\text{-}crystal}$[d]
10	PnDMA	Poly(*n*-decyl methacrylate)	226	782	3.8	–	0	0	0	0	0	10
12	PnLMA	Poly(*n*-lauryl methacrylate)	254	502	4.0	−26	9	2	6	14	0.7	11.3
16	PnHDMA	Poly(*n*-hexadecyl methacrylate)	310	161	2.4	16	39	12	22	39	3.5	12.5
18	PnODMA	Poly(*n*-octadecyl methacrylate)	338	514	4.6	27	46	16	26	≈50[e]	4.7	13.3

[a] T_M as obtained from the maximum of the melting peak.
[b] Determined using $\Delta H = 3.4$ kJ/mol per CH_2 unit of the alkyl rest according to the value estimated for alkanes in [41].
[c] CH_2 (mol%) units in the alkyl nanodomains.
[d] Estimated from D_{cal}: $C = C_{crystal} + C_{non\text{-}crystal}$ with $C_{crystal}$ and $C_{non\text{-}crystal}$ being the numbers of alkyl carbons in crystalline and non-crystalline regions of the alkyl nanodomain, respectively (Fig. 8A).
[e] From [13].

measurement was done during heating after cooling with a rate of about −10 K/min. Temperature steps of 5 K were used corresponding to an average heating rate of +0.3 K/min. The data were fitted using the Havriliak Negami (HN) function $\varepsilon^* = \varepsilon'(\omega) - i\varepsilon''(\omega) = \Delta\varepsilon(1 + (i\omega/\omega_c)^{\beta})^{-\gamma} + \varepsilon_\infty$ and, if required, an additional conductivity term $\sigma \sim 1/\omega$. The fit program [40] uses the Levenberg–Marquardt algorithm for optimization.

3. Results

The standard DSC melting curves for higher poly(*n*-alkyl methacrylates) in Fig. 2 show a systematic increase of the melting peak area with increasing side chain length accompanied by an increase of the (melting) peak temperature T_M. First indications for a crystallization of alkyl rests within alkyl nanodomains are observed for poly(*n*-lauryl methacrylate) with $C = 12$ alkyl carbons per side chain. The increase of the peak area reflects an increase of melting enthalpy ΔH and degree of crystallization D_{cal} while the smaller peak width can be understood as indication for an increasing perfection of the crystalline regions. Analyzing the melting peaks using the simple procedure in the inset of Fig. 2, we observed an increase of the melting enthalpy from $\Delta H \approx 2$ kJ/mol for $C = 12$, $\Delta H \approx 16$ kJ/mol for poly(*n*-octadecyl methacrylate), $C = 18$. This corresponds (Table 1) to an increase of the degree of crystallization from $D_{cal} \approx 6$ to 26 mol% of the alkyl rests considering the approximation

$$D_{cal} = \frac{\Delta H}{\Delta H_{CH_2}} \quad (1)$$

with $\Delta H_{CH_2} \approx 3.4$ kJ/mol being an average melting enthalpy per CH_2 unit for alkanes [41]. Slightly larger values ($\Delta H_{CH_2} \approx 4.1$ kJ/mol) are reported for polyethylene [42]. This causes an uncertainty in the D_{cal} values of about 20% indicated by error bars in Fig. 7.

Typical changes during isothermal crystallization are shown in Fig. 3: standard DSC heating curves for

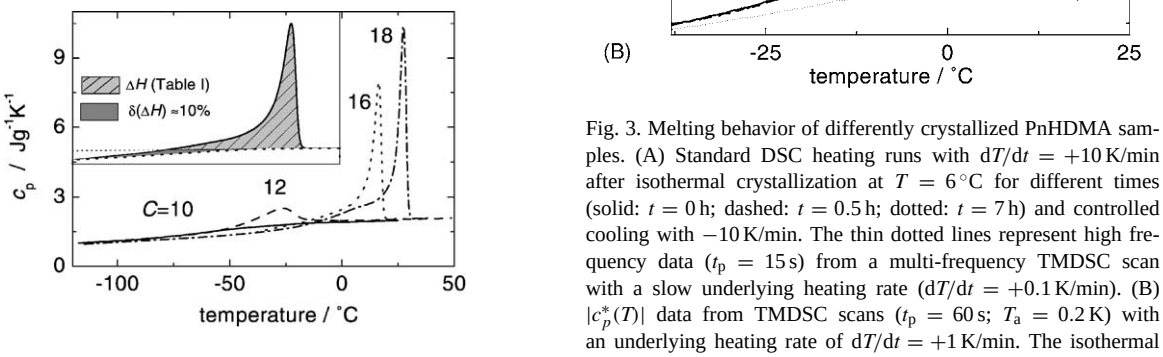

Fig. 2. Standard DSC heating runs with $dT/dt = +10$ K/min after cooling with $dT/dt = -10$ K/min for higher PnAMA. The labels indicate the *C* number. The inset shows the determination of the melting enthalpy ΔH based on an extrapolation of $c_p^{melt}(T)$ and an estimation of the uncertainty $\delta(\Delta H)$ based on high frequency data (thin dotted line) as obtained from multi-frequency TMDSC experiments (Fig. 3).

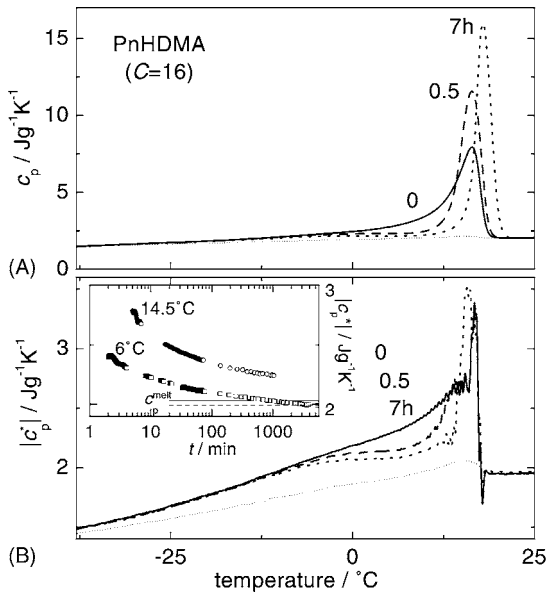

Fig. 3. Melting behavior of differently crystallized PnHDMA samples. (A) Standard DSC heating runs with $dT/dt = +10$ K/min after isothermal crystallization at $T = 6$ °C for different times (solid: $t = 0$ h; dashed: $t = 0.5$ h; dotted: $t = 7$ h) and controlled cooling with −10 K/min. The thin dotted lines represent high frequency data ($t_p = 15$ s) from a multi-frequency TMDSC scan with a slow underlying heating rate ($dT/dt = +0.1$ K/min). (B) $|c_p^*(T)|$ data from TMDSC scans ($t_p = 60$ s; $T_a = 0.2$ K) with an underlying heating rate of $dT/dt = +1$ K/min. The isothermal crystallization times at $T = 6$ °C are the same as in part A. Cooling rate was −10 K/min. The inset shows TMDSC data during the isothermal crystallization at $T = 6$ and 14.5 °C ($t_p = 120$ s; $T_a = 0.4$ K) and the corresponding value of c_p^{melt} ((– – –) $T = 6$ °C; (—) $T = 14.5$ °C) linearly extrapolated from the melt c_p above 20 °C. The isothermal measurement at 14.5 °C was performed on a sample having the some history as the dashed curves in part B.

PnHDMA ($C = 16$) after 0, 0.5 and 7 h isothermal crystallization at 6 °C are presented (Fig. 3A). Obviously, isothermal crystallization causes narrowing and high-temperature shift of the melting peak. Peak area and degree of crystallization, however, are nearly unaffected ($\Delta H \approx 12.3 \pm 0.6$ kJ/mol). Corresponding results from TMDSC (Fig. 3B) show that isothermal crystallization at 6 °C affects mainly the absolute value of the dynamic heat capacity $|c_p^*|$ in the temperature range −10 to 10 °C while $|c_p^*|$ at lower temperatures is nearly unaffected. The comparison with high frequency data ($t_p = 15$ s) from multi-frequency TMDSC measurements indicates that there are contributions due to reversible melting in PnHDMA. The inset of Fig. 3B shows the time dependence of $|c_p^*|$ from TMDSC during the isothermal crystallization at $T = 6$ and 14.5 °C. A comparison with the c_p^{melt} value from an extrapolation of the temperature dependence of c_p in the melt indicates that there are at least in the 14.5 °C experiment contributions due to reversible melting. Obviously, the $|c_p(t)^*|$ value from TMDSC is also in the extrapolation to long times larger than c_p^{melt}.

Assuming that a $|c_p^*|$ curve at higher frequency, e.g. from multi-frequency TMDSC measurements, gives a more realistic baseline for the calculation of the melting enthalpy, the ΔH values could be about 10% larger than those from our standard procedure (inset Fig. 2). However, there will be also uncertainties if single $|c_p^*|$ curves at higher frequencies are known due to the onset of crystallization above $T_g(\alpha_{PE})$. Independent information about the relaxation behavior at TMDSC frequencies for the higher PnAMA ($C \geq 12$) requires experiments in the completly amorphous material close to $T_g(\alpha_{PE})$. The frequency dependence of the underlying dynamic glass transition(s) is not easily to obtain. That there are significant, frequency-dependent contributions to $|c_p^*|$ in the range −40 to 10 °C can be seen by comparing low frequency TMDSC data ($t_p = 60$ s) with data at higher frequency from multi-frequency TMDSC measurements ($t_p = 15$ s) on PnHDMA (Fig. 3B). The assignment of heat capacity contributions to reversible melting and the two dynamic glass transitions in nanophase-separated side chain polymers, however, remains very difficult and is probably impossible based on DSC and TMDSC data alone.

Additional information comes from dielectric measurements during the crystallization of PnHDMA. The

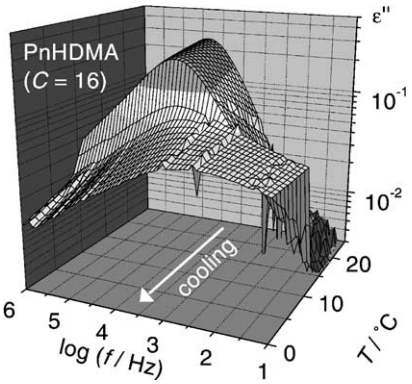

Fig. 4. Imaginary part of the dielectric function, for PnHDMA as obtained in a cooling experiment. The isotherms are measured from 25 to 0 °C every 1 K with an average cooling rate of about $dT/dt = -0.1$ K/min.

imaginary part of the dielectric function ε'' in Fig. 4 was measured during a stepwise cooling of the sample with an effective cooling rate $dT/dt \approx -0.1$ K/min. As the temperature approaches $T_c \approx 11$ °C the sample crystallizes rapidly. This results in a significant broadening of the dielectric loss peak and especially in the occurrence of a low frequency wing. Above and below 11 °C the peak shape is nearly temperature independent. The change of the peak shape is accompanied by a significant decrease of maximum frequency ω_{max} (Fig. 5A) and dielectric relaxation strength $\Delta\varepsilon$ (Fig. 5B). The lower intensity $\Delta\varepsilon$ might be interpreted as a reflection of the decreasing fraction of amorphous material while the peak broadening can be understood as indication of an increasing heterogeneity in the vicinity of the dipoles. One should keep in mind that dielectric spectroscopy detects here mainly the conventional glass transition (a or α) and that the contributions of the polyethylene-like glass transition (α_{PE}) to $\Delta\varepsilon$ are negligible ($\Delta\varepsilon_{\alpha_{PE}}/\Delta\varepsilon_{\alpha} < 0.1$) [25]. Thus, the decrease in $\Delta\varepsilon$ during the crystallization is not a trivial effect but shows clearly the influence of side chain crystallization within the alkyl nanodomains on the main chain, especially the carboxyl group, including the main dipole moment of the monomeric unit.

Considering that the number of mobile dipoles is a measure of the amorphous volume fraction, the degree of crystallization can be estimated [13] from

$$D_\varepsilon(T) = 1 - \left(\frac{\Delta\varepsilon_{sc}(T)}{\Delta\varepsilon_{nc}(T)}\right) \quad (2)$$

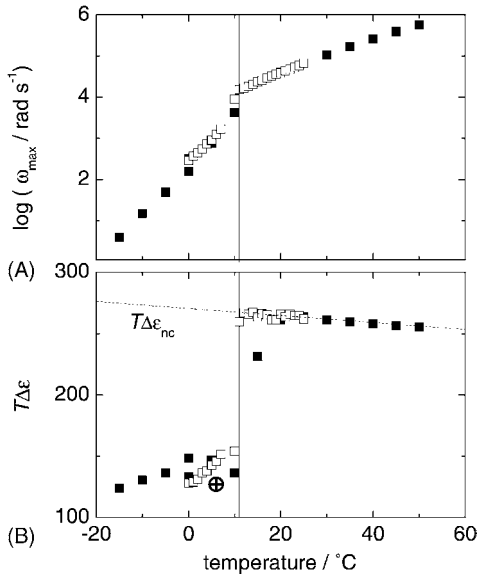

Fig. 5. Frequency of the dielectric loss maximum $\log \omega_{max}$ (A) and relaxation strength $T\Delta\varepsilon$ (B) as function of temperature. Data for two different average cooling and heating rates are shown ((■) −0.1 K/min, (□) +0.3 K/min after rapid cooling with $dT/dt \approx -10$ K/min). The state after isothermal crystallization at 6 °C for 20 h is also given (⊕). The solid line indicates the onset of crystallization at $T_c = 11$ °C, the dotted line is an extrapolation of $\Delta\varepsilon(T)$ in the melt to the temperature range where crystallization occurs.

with $\Delta\varepsilon_{sc}$ and $\Delta\varepsilon_{nc}$ being the dielectric relaxation strength in the semicrystalline and non-crystalline state, respectively. The $\Delta\varepsilon_{nc}(T)$ values are determined by an extrapolation of the dielectric relaxation strength in the melt (Fig. 5B). The $\Delta\varepsilon_{sc}(T)$ values depend significantly on temperature and time-temperature program (Fig. 6). A linear extrapolation of the temperature-dependent $D_\varepsilon(T)$ values, however, gives relatively independent $D_\varepsilon(T_c) \approx 0.39$ values, i.e. the part of the sample that crystallizes spontaneously and fast near T_c is relatively program independent. The $D_\varepsilon(T_c)$ values are compared with the calorimetric D_{cal} values from standard DSC measurements for higher PnAMA in Fig. 7. Obviously, the $D_\varepsilon(T_c)$ values are significantly larger than the corresponding D_{cal} values. This shows the limitations as well as the chances of a combination of both methods. The discrepancy between D_ε and D_{cal} indicates a different influence of the side chain crystallization on calorimetric and dielectric responses. The melting

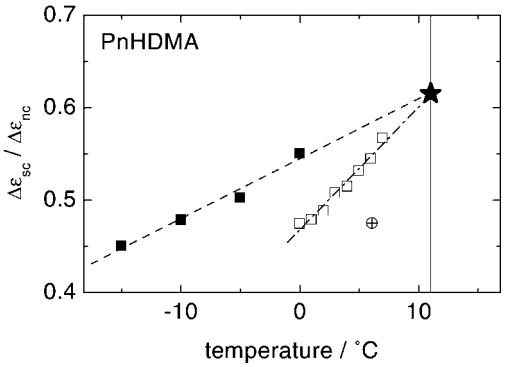

Fig. 6. Temperature dependence of the ratio $\Delta\varepsilon_{sc}/\Delta\varepsilon_{nc}$ in the semicrystalline state of PnHDMA. The samples are crystallized under different conditions (symbols and programs same as in Fig. 5). The dashed lines are linear fits. The state after 20 h isothermal crystallization at $T = 6$ °C (⊕) and the ratio at the onset of crystallization are indicated (★).

enthalpy ΔH should reflect really the contributions from crystalline regions. The simplest explanation for the relation $D_\varepsilon > D_{cal}$ might be the existence of extended rigid amorphous regions. Otherwise, it is not a priori clear why in side chain polymers the polarization fluctuations measured by $\Delta\varepsilon$ should be proportional to the degree of crystallization as suggested by Eq. (2). Nevertheless, a comparison of both values, D_ε and D_{cal}, should help to learn more about the morphology of nanophase-separated polymers as well as about importance and content of rigid amorphous or pre-ordered regions in

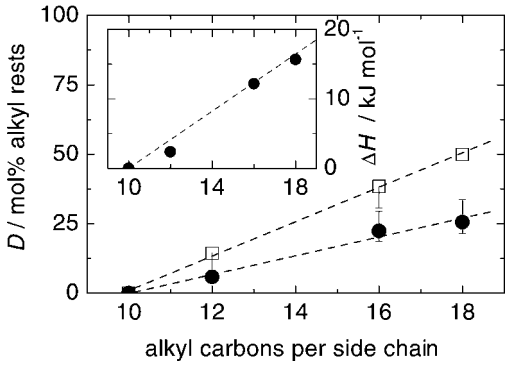

Fig. 7. Degree of crystallization D and melting enthalpy ΔH (inset) as obtained for several higher PnAMA from calorimetry ((●) D_{cal}, Eq. (1)) and dielectrics ((□) D_ε, Eq. (2)).

semicrystalline materials, especially within alkyl nanodomains.

The increase of ΔH and D_{cal} with the number of alkyl carbons is nearly linear (Fig. 7). This suggests [13,43,44] a simple morphological picture as shown in Fig. 8A. Following this picture the number of non-crystalline carbons per side chain C_{nc} is nearly constant (Table 1), i.e. a approximately fixed number of alkyl carbons close to the backbones are not able to crystallize. It is interesting that all lower PnAMA ($C < 12$), where the conventional glass temperature involving the main chain is significantly higher than $T_g(\alpha_{PE})$, do not crystallize. If $T_g(\alpha)$ approaches $T_g(\alpha_{PE})$ ($C \approx 12$, Fig. 1B) side chain crystallization starts to occur. Similar behavior is indicated for other series of side chain polymers with alkyl rests and more or less flexible backbones [45]. This may indicate that frustration introduced by the main chain is an important factor for the ability of alkyl rests to orientate and crystallize in the alkyl nanodomains.

Fig. 7 shows also that D_{cal} and the dielectric degree of crystallization close to T_c, $D_\varepsilon(T_c)$, are surprisingly proportional to each other. This is somehow unexpected in the quasi one-dimensional picture (Fig. 8A) because the number of non-crystalline alkyl carbons is nearly constant and unaffected by the side chain length if we apply this picture to our data. Nevertheless, the dielectric relaxation strength $\Delta\varepsilon$ related to the dipoles in the direct vicinity of the non-crystalline parts of the alkyl rest is proportional to the number of crystalline alkyl carbons C_{cryst}. One may argue that the change in $\Delta\varepsilon$ has to do with rigid amorphous parts of the alkyl rest. The proportionality $D_\varepsilon \propto D_{cal}$, however, is not straight forward in this picture. The good agreement between melting temperatures of alkyl rests in higher PnAMA and alkanes with the same number of alkyl carbons (Fig. 1B) is another point that is not so easy to explain in this picture. The observed coincidence suggests intuitively that the alkyl rests are completely incorporated in a crystalline region.

An alternative, more global picture (Fig. 8B) is the view that only a certain fraction of the alkyl nanodomains will crystallize. In this heterogeneous picture it seems more logical that D_ε is proportional to D_{cal} and that the T_M values for alkanes and alkyl rests are very similar. However, this picture can not explain easily the linear dependence of D_{cal} and C_{cryst} on the side chain length. In any case, the situation in semicrystalline side chain polymers should be characterized by some spatial heterogeneity not included in the simple one-dimensional picture (Fig. 8A) and the real morphology of such systems should be somewhere in-between the two extremes discussed above (Fig. 8A and B).

Looking on structural data from X-ray scattering [22] for PnAMA in the amorphous (glassy for $C < 4$ or molten for $C \geq 4$) state at $T = 25\,^\circ C$ (Fig. 1A) we can also not decide between the two alternatives in Fig. 8. Obviously, significant changes occur near $C = 12$ although the studied polymers are in the non-crystalline state during the scattering experiments ($T_M \leq 25\,^\circ C$, Table 1). The equivalent Bragg spacing

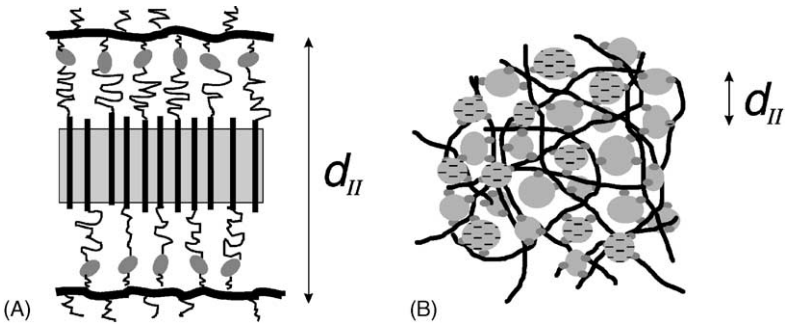

Fig. 8. Schematic representation of a quasi one-dimensional model (A) and a more global three-dimensional picture (B) for the morphology of nanophase-separated side chain polymers. The repeating distance d_{II} reflected by a pre-peak in X-ray scattering data (Fig. 1A) is indicated. (A) The bold lines represent the backbones, the crystalline region is shown in gray, the thin lines are amorphous or rigid amorphous parts of the alkyl rest. (B) The backbones are the bold lines and the gray regions are aggregated alkyl rests. The hatching indicates crystalline regions. In both parts, the small ellipses represent the dipoles in the carboxyl groups.

related to the pre-peak shows a step from $d_{II} = 1.9$ to 2.5 nm and a change in the C number dependence is indicated. Intuitively it is clear is that a transition from separated alkyl nanodomains to a continuous phase should occur with increasing C number due to the increasing volume fraction of the alkyl rests. If the observed changes in d_{II} have to do with such an effect is not yet clear. Probably the $d_{II}(C)$ dependence below $C = 12$ is non-linear [24], i.e. not consistent with an all *trans* configuration of the alkyl rests. The difference between the Bragg spacings for PnODMA in the molten and semicrystalline state, however, is obviously relatively small indicating a high degree of internal order within the alkyl nanodomains also in the molten state without indications of crystalline order in X-ray scattering data [22]. A significant broadening of the pre-peak in the range $6 \leq C \leq 12$ could be interpreted as superposition of two contributions in this region. One could speculate about the coexistence of amorphous and pre-ordered amorphous or crystalline regions as observed for other side chain polymers with long alkyl rests by NMR [44]. This would support spatial heterogeneity in the sense of Fig. 8B. However, final statements about the existence of pre-ordered states can not be made based on our X-ray scattering data and further information about the morphology of nanophase-separated side chain polymers are needed.

4. Discussion

Summarizing all the experimental findings for our series of atactic PnAMA, the situation can be discussed consistently in the following context. Nanophase separation of incompatible main and side chain parts starts already in the lower amorphous members ($4 \leq C < 12$) and leads to the coexistence of two dynamic glass transitions, a or α and α_{PE}. The polyethylene-like glass transition α_{PE} occurs within alkyl nanodomains formed by aggregated alkyl rests. This underlines a certain independence of the dynamics within these domains. The glass temperature $T_g(\alpha_{PE})$ increases systematically with side chain length and alkyl domain size. Obviously, the short alkyl rests are not able to crystallize close to the less mobile main chain. If the side chains are long and flexible enough ($C \geq 12$) and the mobility of the main chain is comparable to that of the alkyl rests, crystallization in the alkyl nanodomains starts to occur. The perfection of the structure inside the alkyl nanodomains increases without basic changes in the nanophase separation of main and side chain parts. For even longer alkyl rests degree of crystallization D_{cal} and melting temperature T_M increase while the dielectric relaxation strength $\Delta\varepsilon$ decreases indicating an immobilization of the main chain due to crystallization in the alkyl nanodomains.

A central question is why the glass temperature in the alkyl nanodomains $T_g(\alpha_{PE})$ increases with side chain length. There are two alternative ideas to explain this. One can think about increasing order in the alkyl nanodomains. It is an old empirical rule that the glass temperature increases with increasing order in the system. Alternatively, one can understand the increase in $T_g(\alpha_{PE})$ as a reflection of the increasing size of the alkyl nanodomains being a self-assembled confinement for the polyethylene-like glass transition in our nanophase-separated systems. An increase of T_g with the size of nanometer confinements is experimentally observed in the amorphous regions of specifically crystallized poly(ethylene terephthalate) (PET) samples [9] and several liquids confined in nanoporous glasses with typical pore sizes in the range 2.5–10 nm [19]. This effect is usually discussed in the picture of a hindered glass transition [46] and related to the interaction between confinement and the size of cooperatively rearranging regions, relevant for the cooperative dynamics in glass-forming materials [32].

Interestingly, the increase in $T_g(\alpha_{PE})$ with C for the amorphous members ($C < 12$) is comparable to increase in T_M with C for the semicrystalline members ($C \geq 12$) (Fig. 1B). If this is true, it seems to be an important question why both dependencies are similar. One could speculate that this is a reflection of a general trend in side chain mobility: In the lower members, the alkyl rests become mobile first but side chain crystallization can not occur due to the frustration by main chains which become mobile at much higher temperatures (mobile alkyl nanodomains in a stiff main chain matrix; Fig. 1B). In the higher members, the onset of crystallization is determined by side chain mobility. Crystallization occurs slightly above the glass temperature of the alkyl nanodomains, $T_g(\alpha_{PE})$, where the alkyl rest become mobile. In this sense, the T_M values would be coupled to the $T_g(\alpha_{PE})$ values and the similarity of the C number dependencies of $T_g(\alpha_{PE})$ and

T_M above and below $C = 12$ would be only consequent. Otherwise, changes in T_M for semicrystalline materials are often discussed to be a result of a variation in the thickness of the crystalline lamella (of the order of 10–30 nm). Especially, the increase in T_M for alkanes was related to the thickness of the lamellae formed by extended molecules in the framework of Gibbs–Thomson-like approaches [41]. This may indicate the general importance of confinement effects in amorphous and semicrystalline systems with structural heterogeneities in the 1–10 nm range.

Qualitatively, our findings concerning the dependence of D_{cal} on the alkyl nanodomain size are consistent with the results of recent studies to the influence of nanometer confinements on the crystallization in microphase-separated block copolymers with domain sizes of about 10 nm. Also in this case the degree of crystallization decreases usually with decreasing domain size [17]. The situation in nanophase-separated side chain polymers is obviously similar but characterized by more topological constraints and smaller domain sizes of order of 1–3 nm. This indicates general aspects in systems with self-assembled nanometer confinements. Due to the smaller domain sizes in nanophase-separated side chain polymers, one would expect that in such systems early stages of crystallization [16] and pre-ordering effects can be observed more clearly. The fact that the alkyl nanodomain size can be tuned precisely and easily by changing the side chain length may offer new possibilities. Side chain polymers enable us to study the crystallization process within alkyl nanodomains not only as function of time and temperature but also depending on domain size and main chain mobility.

5. Conclusions

We have shown that a nanophase separation of incompatible main and side chain parts is a characteristic feature of both—amorphous and semicrystalline—PnAMA. The common aspect is the existence of alkyl nanodomains with a typical dimension of order 1–3 nm. Within these nanodomains, a crystallization of alkyl rests occurs for the higher members while an independent polyethylene-like glass transition α_{PE} is observed in lower members. Comparing our results from calorimetry and dielectrics with the predictions of different morphological pictures, we conclude that neither a simple quasi one-dimensional picture nor an oversimplified three-dimensional picture can explain all the experimental findings in a consistent way. Probably the real morphology of nanophase-separated side chain polymers combines certain aspects of both pictures. Two alternative explainations for a comparable increase in $T_g(\alpha_{PE})$ and T_M with side chain length (C number) in amorphous and semicrystalline poly(n-alkyl methacrylates) are considered. The first interpretation is based on orientation arguments, the second on confinement effects. The increase in $T_g(\alpha_{PE})$ is either related to an increasing order within alkyl nanodomains or discussed in terms of a hindered glass transition in a self-assembled nanometer confinement. The T_M shift could be a consequence of the increase in $T_g(\alpha_{PE})$, i.e. caused by side chain mobility, or related to spatial aspects, i.e. due to the increasing lamella thickness following Gibbs–Thomson-like approaches. In general, the presented results indicate the importance of spatial nanoheterogeneities for a better understanding of the properties of semicrystalline and amorphous side chain polymers.

Acknowledgements

The authors thank D. Sukhorukov and Prof. C. Schick (Rostock) for performing multi-frequency TMDSC measurements, Dr. K. Schröter for helpful discussions, and Dr. S. Höring (Halle) for providing several PnAMA samples. Financial support by the Deutsche Forschungsgemeinschaft DFG (SFB 418) is acknowledged.

References

[1] S.S. Rogers, L. Mandelkern, J. Chem. Phys. 61 (1957) 985.
[2] R. Hoffmann, W. Kappe, Kolloid Z.-Z. Polym. 247 (1971) 763.
[3] J.D. Ferry, Viscoelastic Properties of Polymers, third ed., Wiley, New York, 1980.
[4] N. McCrum, B. Read, G. Williams, Anelastic and Dielectric Effects in Polymeric Solids. Wiley, London, 1967.
[5] J. Heijboer, Mechanical properties and molecular structure of organic polymers, in: J.A. Prins (Ed.), Physics of Non-crystalline Solids, North-Holland, Amsterdam, 1965, pp. 231–253.
[6] R.L. Miller, R.F. Boyer, J. Heijboer, J. Polym. Sci., Polym. Phys. Ed. 22 (1984) 2021.

[7] B. Wunderlich, Macromolecular Physics, Academic Press, New York, 1980.
[8] G. Strobl, The Physics of Polymers, Springer, Berlin, 1996.
[9] C. Schick, E. Donth, Phys. Scripta 43 (1991) 423.
[10] A. Nogales, T.A. Ezquerra, F. Batallan, B. Frick, E. Lopez-Cabarcos, F.J. Balta-Calleja, Macromolecules 32 (1999) 2301.
[11] T.A. Ezquerra, I. Sics, A. Nogales, Z. Denchev, F.J. Balta-Calleja, Europhys. Lett. 59 (2002) 417.
[12] B. Wunderlich, Prog. Colloid Polym. Sci. 96 (1994) 22.
[13] M. Mierzwa, G. Floudas, P. Stepanek, G. Wegner, Phys. Rev. B 62 (2000) 14012.
[14] J. Mijovic, J.W. Sy, Macromolecules 35 (2002) 6370.
[15] W. Chen, B. Wunderlich, Macromol. Chem. Phys. 200 (1999) 283.
[16] G. Strobl, Eur. Phys. J. E 3 (2000) 165.
[17] I.W. Hamley, The Physics of Block Copolymers, Oxford University Press, Oxford, 1998.
[18] J.A. Forrest, J. Mattsson, Phys. Rev. E 61 (2000) R53.
[19] M. Arndt, R. Stannarius, H. Groothues, E. Hempel, F. Kremer, Phys. Rev. Lett. 79 (1997) 2077.
[20] M. Beiner, K. Schröter, E. Hempel, S. Reissig, E. Donth, Macromolecules 32 (1999) 6278.
[21] G. Floudas, P. Stepanek, Macromolecules 31 (1998) 6951.
[22] S. Reichl, O. Kabisch, H. Huth, et al., to be published.
[23] J. dAns, E. Lax, Taschenbuch für Chemiker und Physiker. Band 2: Organische Verbindungen, fourth ed., Springer, Berlin, 1983.
[24] M. Beiner, Macromol. Rapid Commun. 22 (2001) 869.
[25] M. Beiner, O. Kabisch, S. Reichl, H. Huth, J. Non-Cryst. Solids 307–310 (2002) 658.
[26] E. Hempel, M. Beiner, H. Huth, E. Donth, Thermochim. Acta 391 (2002) 219.
[27] J.M.G. Cowie, Z. Haq, I.J. McEwen, J. Velickovic, Polymer 22 (1981) 327.
[28] K.W. McCreight, J.J. Ge, M. Guo, I. Mann, F. Li, Z. Shen, X. Jin, F.W. Harris, S.Z.D. Cheng, J. Polym. Sci. B: Polym. Phys. 37 (1999) 1633.
[29] C. Schick, A. Wurm, A. Mohamed, Colloid Polym. Sci. 279 (2001) 800.
[30] B. Wunderlich, Prog. Polym. Sci. 28 (2003) 383.
[31] G. Adam, J.H. Gibbs, J. Chem. Phys. 43 (1965) 139.
[32] E. Donth, H. Huth, M. Beiner, J. Phys.: Condens. Matter 13 (2001) L451.
[33] A. Heuer, H.W. Spiess, Phys. Rev. Lett. 82 (1999) 1335.
[34] A. Arbe, J. Colmenero, M. Monkenbusch, D. Richter, Phys. Rev. Lett. 82 (1999) 1336.
[35] S.M. Sarge, W. Hemminger, E. Gmelin, G.W.H. Höhne, H.K. Cammenga, W. Eysel, J. Thermal Anal. 49 (1997) 1125.
[36] A. Hensel, C. Schick, Thermochim. Acta 304–305 (1997) 229.
[37] C. Schick, U. Jonsson, T. Vassiliev, A. Minakov, J. Schawe, R. Scherrenberg, D. Lörinczy, Thermochim. Acta 347 (2000) 53.
[38] S. Weyer, A. Hensel, C. Schick, Thermochim. Acta 304/305 (1997) 267.
[39] M. Merzlyakov, C. Schick, Thermochim. Acta 377 (2001) 193.
[40] K. Schröter, R. Unger, S. Reissig, F. Garwe, S. Kahle, M. Beiner, E. Donth, Macromolecules 31 (1998) 8966.
[41] G. Höhne, Polymer 43 (2002) 4689.
[42] Advanced THermal Analysis System (ATHAS): Wunderlich, B. Pure Appl. Chem. 1995, 67, 1919; see also: http://www.web.utk.edu/athas.
[43] V. Arrighi, A. Triolo, I.J. McEwen, P. Holmes, R. Triolo, H. Amenitsch, Macromolecules 33 (2000) 4989.
[44] J. Clauss, K. Schmidt-Rohr, A. Adam, C. Boeffel, H.W. Spiess, Macromolecules 25 (1992) 5208.
[45] M. Beiner, H. Huth, submitted for publication.
[46] E. Donth, Glasübergang, Akademie-Verlag, Berlin, 1981.